

co-BPM: a Bayesian Model for Divergence Estimation

Kun Yang¹, Hao Su², and Wing Hung Wong³

¹Institute of Computational and Mathematical Engineering, Stanford University

²Department of Computer Science, Stanford University

³Department of Statistics, Stanford University

³Department of Health Research and Policy, Stanford University

Abstract

Divergence is not only an important mathematical concept in information theory, but also applied to machine learning problems such as low-dimensional embedding, manifold learning, clustering, classification, and anomaly detection. We proposed a bayesian model—co-BPM—to characterize the discrepancy of two sample sets, i.e., to estimate the divergence of their underlying distributions. In order to avoid the pitfalls of plug-in methods that estimate each density independently, our bayesian model attempts to learn a coupled binary partition of the sample space that best captures the landscapes of both distributions, then make direct inference on their divergences. The prior is constructed by leveraging the sequential buildup of the coupled binary partitions and the posterior is sampled via our specialized MCMC. Our model provides a unified way to estimate various types of divergences and enjoys convincing accuracy. We demonstrate its effectiveness through simulations, comparisons with the *state-of-the-art* and a real data example.

Key Words: coupled binary partition, divergence, MCMC, clustering, classification

1 Introduction

Divergence between two distributions is of significant importance in various disciplines such as statistics, information theory and machine learning. In statistics, hypothesis testing procedures such as Kolmogorov-Smirnov test and Cramer-von Mises test are based on some discrepancy measurements of the empirical distributions, and a common goal in bayesian

experimental design (Chaloner and Verdinelli, 1995) is to maximize the expected Kullback-Leibler (KL) divergence between the prior and the posterior. In information theory, theoretic quantities such as mutual information and Shannon Entropy are derived from divergences. In machine learning, different divergences such as Total Variation, Hellinger Distance and KL divergence are often applied as a dissimilarity measure in manifold learning (Donoho and Grimes, 2003), classification and anomaly detection, etc. Recently, they are also applied to developing efficient methods for a robust empirical risk minimization problem (Namkoong and Duchi, 2016).

Given two probability measures P_1 and P_2 defined on domain Ω , we consider the case that P_1 and P_2 have their densities p_1 and p_2 , a general form of divergence is given by

$$D_\phi(p_1, p_2) = \int p_1(x) \phi\left(\frac{p_2(x)}{p_1(x)}\right) dx$$

where ϕ is a convex function. D_ϕ is the class of Ali-Silvey distances (Ali and Silvey, 1966), also known as f -divergences. Many common divergences, such as KL divergence ($\phi(x) = -\log(x)$), α -divergence (e.g., $\phi(x) = 4/(1 - \alpha^2) \cdot (1 - x^{(\alpha+2)/2})$ when $\alpha \neq \pm 1$), Hellinger distance ($\sqrt{D_\phi}$ and $\phi(x) = 1 - \sqrt{x}$), and total variation distance ($\phi(x) = |x - 1|$), are special cases of f -divergence, coinciding with a particular choice of ϕ .

We are interested in estimating D_ϕ from two sample sets \mathcal{X} and \mathcal{Y} , where $\mathcal{X} = \{x_i\}_{i=1}^{n_1}$ and $\mathcal{Y} = \{y_i\}_{i=1}^{n_2}$ are iid samples drawn from P_1 and P_2 respectively. A conceptually simple approach proceeds in two-steps: estimate the densities \hat{p}_1 and \hat{p}_2 with \mathcal{X} and \mathcal{Y} independently then calculate $D_\phi(\hat{p}_1, \hat{p}_2)$. However, this approach is unattractive for the following reasons: 1) multivariate density estimation itself is a challenging problem and often more difficult than comparing distributions, poorly estimated densities lead to high variance and bias in subsequent divergence estimation (Ma and Wong, 2011); 2) with \hat{p}_1 and \hat{p}_2 estimated independently, we are often unable to compute their divergence $D_\phi(\hat{p}_1, \hat{p}_2)$ analytically, and the application of numeric or approximation methods introduces additional error terms (Sugiyama et al., 2012). Hence, throughout this paper, we focus on the class of single-shot methods, i.e., comparing sample sets directly and simultaneously.

Divergence estimation, especially KL divergence, has a long history and rich literature, we review several methods in the context of information theory and machine learning. Interested readers may refer to (Sricharan et al., 2010; Wang et al., 2009; Leonenko et al., 2008; Póczos and Schneider, 2011; Ma and Wong, 2011; Póczos et al., 2012) for other recent developments. (Wang et al., 2005) proposes a domain-partitioning method that constructs an adaptive partition of the sample space with respect to \mathcal{Y} , then Radon-Nikodym derivative $p_1(x)/p_2(x)$ can be estimated with empirical probability mass (with the correction term on the boundary) in each sub-region. In 1-dimension, strong consistency is established and several algorithmic refinements are suggested. In multi-dimensions, a partitioning scheme is also mentioned based on the heuristics in 1-dimensional case, however, there are not enough

numeric simulations to justify the heuristics. (Nguyen et al., 2010) derives a variational characterization of the f -divergence in terms of a bayes decision problem, which is exploited to develop an M -estimator. The theoretical results of consistency and convergence rates are provided. It is also shown that the estimation procedure can be cast into a finite-dimensional convex program and solved efficiently when the functional class is defined by reproducing kernel Hilbert spaces. (Sugiyama et al., 2012) introduces the least-squares density-difference estimator developed under the framework of kernel regularized least-squares estimation. The finite sample error bound shows that it achieves the optimal convergence rate. They also demonstrate several pattern recognition applications.

Despite of the success of these methods, they are insufficient in several scenarios. Firstly, since \mathcal{X} and \mathcal{Y} are two sets of random samples, one may be interested in the confidence (credible) intervals of estimated divergences (Sricharan et al., 2010), but deriving such quantities are non-trivial for these methods. Secondly, these methods and theories are all set up for a specific type of divergence and are usually not directly applicable to others. Thirdly, based on our practical experience, previous work (Sricharan et al., 2010; Nguyen et al., 2010; Pérez-Cruz, 2008) faces challenges to scale to higher dimensions, even though most of the methods claim that there are no technical difficulties as the number of dimensions increases.

In this paper, we introduce a single-shot bayesian model, which we name as **coupled Binary Partition Model** (co-BPM). Our model is inspired by two key ideas. Firstly, we use an adaptive partitioning scheme, which has been demonstrated to be more scalable (see Table 1) than traditional domain-partitioning methods such as histogram (Wang et al., 2005) or regular paving (Sainudiin et al., 2013). Secondly, instead of partitioning based upon \mathcal{Y} alone as in (Wang et al., 2005), we force the domain Ω to be *coupled* so that it is partitioned with respect to \mathcal{X} and \mathcal{Y} simultaneously. Therefore, our model is capable of capturing the landscapes of both \mathcal{X} and \mathcal{Y} , thus is more effective in estimating their divergences.

We highlight our contributions as follows:

1. co-BPM is a *single-shot domain-partition* based bayesian model for divergence estimation, that is scalable in both dimension and sample size.
2. Our specifically tailored MCMC sampling algorithm exploits the sequential buildup of binary partition for rapid mixing.
3. co-BPM enjoys convincing accuracy and demonstrates superior performance in machine learning tasks such as clustering and classification.

We validate our model by several examples: 1) two sanity tests to demonstrate that our model is sensitive to the differences among samples; 2) 1-dim and 3-dim numeric examples to assess the estimation accuracies; 3) simulations in 3-dim used to compare with the *state-of-the-art* such as (Nguyen et al., 2010) and (Pérez-Cruz, 2008); 4) real data applications to image clustering and classification.

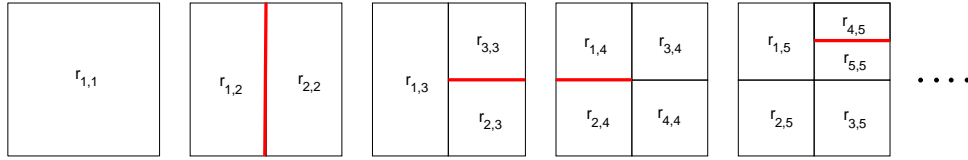


Figure 1: A **binary partition sequence** demonstrates its sequential structure. Each red line indicates the decision to halve the sub-region along it.

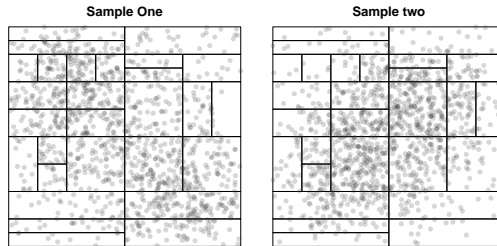


Figure 2: An illustration of **coupled binary partition** of two samples through the coupled binary partition model. Two samples are drawn from two different distributions and their sampling spaces are partitioned in tandem.

The rest of the paper is organized as follows: Section 2 introduces some notations used throughout our discussion and preliminaries that motivate our model; Section 3 introduces the Coupled Binary Partition Model and the specially tailored MCMC algorithm to sample posterior effectively; extensive simulations and comparisons are presented in Section 4; we draw the conclusions in Section 5.

2 Notation and Preliminaries

Without loss of generality, we assume the domain $\Omega = [0, 1]^d$ with dimension d . A coordinate-wise binary partition has hierarchical structure that is constructed sequentially (Figure 1 gives an illustration of the sequence in $[0, 1]^2$): starting with $\mathcal{B}_1 = \{r_{1,1} = \Omega\}$ at depth 1, action a_1 is taken to split Ω into $\mathcal{B}_2 = \{r_{1,2}, r_{2,2}\}$ along the middle of some coordinate; then at depth 2, action a_2 is taken to halve some sub-region in \mathcal{B}_2 into $\mathcal{B}_3 = \{r_{1,3}, r_{2,3}, r_{3,3}\}$ evenly. The process keeps on till the specified depth is reached. Given the maximum depth l , the decision sequence is denoted as $A_l = (a_1, \dots, a_{l-1})$. A_l uniquely determines a partition of Ω , whose sub-regions are denoted as $\{r_{1,l}, \dots, r_{l,l}\}$. It is necessary to point out that different decision sequences may result in the same partition. Figure 2 demonstrates the coupled binary partition, where the domains of two different sample sets are partitioned in tandem. The following property and theorem motivate us to construct co-BPM.

Property 1. For any pair of decision sequences A_{l_1} and A_{l_2} and their partitions $\{r_{i_1, l_1}\}_{i_1=1}^{l_1}$ and $\{r_{i_2, l_2}\}_{i_2=1}^{l_2}$, there exists a sequence A_l and its partition $\{r_{i, l}\}_{i=1}^l$ such that r_{i_k, l_k} is the union of a subset of $\{r_{i, l}\}_{i=1}^l$ for $k = 1, 2$ and $i_k = 1, \dots, l_k$, namely, A_l defines a finer partition than A_{l_1} and A_{l_2} .

The next theorem shows that a partition of Ω gives a lower bound of the discrepancies.

Theorem 1. Given a partition $\{r_{1, l}, \dots, r_{l, l}\}$ of Ω at depth l , let

$$\tilde{p}_i(x) = \sum_{k=1}^l \frac{P_i(r_{k, l})}{|r_{k, l}|} \mathbf{1}\{x \in r_{k, l}\}$$

where $i = 1, 2$ and $|\cdot|$ denotes the volume or size, then

$$D_\phi(p_1, p_2) \geq D_\phi(\tilde{p}_1, \tilde{p}_2) \quad (1)$$

namely, a partition gives a way to estimate D_ϕ .

Remark 2.1. Another lower bound (Nguyen et al., 2010) of D_ϕ is $\sup_{f \in \mathcal{F}} \int [fdP_2 - \phi^*(f)dP_1]$, where \mathcal{F} is a class of functions and ϕ^* is the conjugate dual function of ϕ . Theorem 1 shifts the difficulty of estimation from finding a good \mathcal{F} to a good partition.

Remark 2.2. Under the condition that the integral $D_\phi(p_1, p_2)$ is Riemann integrable. It is trivial to show that $D_\phi(p_1, p_2) = \sup D_\phi(\tilde{p}_1, \tilde{p}_2)$, where the supremum is taken over all possible partitions at all depths.

The proof is straightforward by applying the Jensen's inequality.

Proof. We decompose the integral by $\{r_{1, l}, \dots, r_{l, l}\}$ and apply Jensen's inequality,

$$\begin{aligned} D_\phi(p_1, p_2) &= \int_{\Omega} p_1(x) \phi\left(\frac{p_2(x)}{p_1(x)}\right) dx = \sum_{i=1}^l \int_{r_{i, l}} p_1(x) \phi\left(\frac{p_2(x)}{p_1(x)}\right) dx \\ &= \sum_{i=1}^l P_1(r_{i, l}) E_{p_1(\cdot|r_{i, l})} \left[\phi\left(\frac{p_2(x)}{p_1(x)}\right) \right] \geq \sum_{i=1}^l P_1(r_{i, l}) \phi\left(E_{p_1(\cdot|r_{i, l})} \frac{p_2(x)}{p_1(x)}\right) = \sum_{i=1}^l P_1(r_{i, l}) \phi\left(\frac{P_2(r_{i, l})}{P_1(r_{i, l})}\right) \end{aligned} \quad (2)$$

□

Theorem 1 provides to a lower bound of f -divergence on finite partitions, Table 1 illustrates the importance of a good partition. Within each region, the gap between $D_\phi(p_1, p_2)$ and $D_\phi(\tilde{p}_1, \tilde{p}_2)$ comes from applying Jensen's inequality, therefore, it can be closed if $p_1(x)/p_2(x)$ in each region is approximately constant. Such observations indicate that finer partition of the domain would reduce the estimation bias. However, an overly fine partition will cause insufficient samples in each sub-region and inadvertently increase the overall estimation variance. So there is a *trade-off between bias and variance*. Therefore, an appropriate partitioning respecting the tradeoff should reflect the landscape of \mathcal{X} and \mathcal{Y} simultaneously and avoid over-cutting. We will see how this intuition is implemented in our bayesian model.

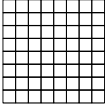
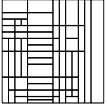
| (i) | | (ii) | | | | | | | | |
|---------------|---------------|---------------|---------------|---|---|-----------|---------------|----------------|----------------|---------------|
| Ω_{12} | Ω_{11} | Ω_{21} | Ω_{22} |  |  | $D_{q=1}$ | $D_{q=2}$ | $D_{\alpha=1}$ | $D_{\alpha=2}$ | |
| | | | | | | Hist | 0.5269 | 0.4935 | 0.7964 | 1.0291 |
| | | | | | | BP | 0.5431 | 0.4990 | 0.8267 | 1.0527 |
| | | | | | | Truth | 0.5518 | 0.5204 | 0.8604 | 1.0769 |

Table 1: **A simple illustration demonstrates the importance of a good partition.** (I) $\mathcal{B}_1 = \{\Omega_{11}, \Omega_{12}\}$ and $\mathcal{B}_2 = \{\Omega_{21}, \Omega_{22}\}$ are two partitions of unit cube. Consider $p_1(x) = \frac{3}{2}\mathbf{1}\{x \in \Omega_{11}\} + \frac{1}{2}\mathbf{1}\{x \in \Omega_{12}\}$ and $p_2(x) = \frac{1}{2}\mathbf{1}\{x \in \Omega_{11}\} + \frac{3}{2}\mathbf{1}\{x \in \Omega_{12}\}$. Under \mathcal{B}_1 , the lower bounds equal $D_\phi(p_1, p_2)$, i.e., $D_\phi = \frac{3}{4}\phi(\frac{1}{3}) + \frac{1}{4}\phi(3)$. For instance, the Total Variation Distance is $\frac{1}{2}$, Hellinger Distance is $\frac{\sqrt{3}}{2} - \frac{1}{2}$ and α -divergence is $\alpha = 2$ is $\frac{1}{\alpha-1} \log(\frac{3}{4} \cdot 3^{\alpha-1} + \frac{1}{4} \cdot \frac{1}{3}^{\alpha-1})$ respectively; however, under \mathcal{B}_2 , the lower bounds are $\phi(1)$, where the Total Variation Distance, Hellinger Distance and α -divergence with $\alpha = 2$ are all 0. (II) $p_1(x) = \beta_{3,5}(x_1)\beta_{3,5}(x_2)$ and $p_2(x) = \mathbf{1}\{x \in [0, 1]^2\}$. On the left is histogram by dividing each dimension into 8 equal sub-intervals; on the right is an adaptive partition with 64 sub-rectangles. As summarized in the right table, **BP** (adaptive binary partition) is closer to **Truth** (the true values) than **Hist** (histogram).

3 Coupled Binary Partition Model

In light of Property 1 and Theorem 1, for a given partition $\{r_{i,l}\}_{i=1}^l$, we approximate the density p_1 and p_2 with \hat{p}_1 and \hat{p}_2 as

$$\hat{p}_1(x) = \sum_{i=1}^l \frac{m_{1i,l}}{|r_{i,l}|} \mathbf{1}\{x \in r_{i,l}\}, \hat{p}_2(y) = \sum_{i=1}^l \frac{m_{2i,l}}{|r_{i,l}|} \mathbf{1}\{y \in r_{i,l}\}$$

where $\sum_{i=1}^l m_{1i,l} = 1$, $\sum_{i=1}^l m_{2i,l} = 1$; $\mathbf{m}_{k,l} = (m_{k1,l}, \dots, m_{kl,l}) \geq \mathbf{0}$, $k = 1, 2$. Based on \hat{p}_1 and \hat{p}_2 , we estimate divergence $D_\phi(p_1, p_2)$ as $D_\phi(\hat{p}_1, \hat{p}_2)$, where

$$D_\phi(\hat{p}_1, \hat{p}_2) = \sum_{i=1}^l m_{1i,l} \phi\left(\frac{m_{2i,l}}{m_{1i,l}}\right) \quad (3)$$

The parameters $\mathbf{m}_{1,l}$, $\mathbf{m}_{2,l}$ and $\{r_{i,l}\}_{i=1}^l$ are unknown, we assign a prior to them as follows: 1) Assume that $\{r_{i,l}\}_{i=1}^l$ is generated by a decision sequence $A_l = (a_1, \dots, a_{l-1})$; 2) A decision sequence of depth $l \in \mathcal{N}^+$ has a prior density proportional to $\exp(-\sigma l)$ with some positive σ and all decision sequences at the same depth are distributed uniformly—this part of the prior is to discourage over-cutting as discussed in the previous section; 3) $\mathbf{m}_{1,l}$, $\mathbf{m}_{2,l}$ have a Dirichlet prior $\text{Dir}(\delta, \dots, \delta)$ respectively with some positive δ and the priors are independent between sample sets \mathcal{X} and \mathcal{Y} . Thus,

$$p(l, A_l, (\mathbf{m}_{1,l}, \mathbf{m}_{2,l})) \propto \exp(-\sigma l) \prod_{i=1}^l m_{1i,l}^{\delta-1} \prod_{i=1}^l m_{2i,l}^{\delta-1}$$

The likelihood of \mathcal{X} and \mathcal{Y} is

$$p(\mathcal{X}, \mathcal{Y} | (l, A_l, (\mathbf{m}_{1,l}, \mathbf{m}_{2,l}))) = \prod_{i=1}^l \left(\frac{m_{1i,l}}{|r_{i,l}|} \right)^{n_{1i,l}} \prod_{i=1}^l \left(\frac{m_{2i,l}}{|r_{i,l}|} \right)^{n_{2i,l}}$$

where $\mathbf{n}_k = (n_{ki,l})_{i=1}^l$, $k = 1, 2$ denote the number of samples in each sub-region with respect to sample sets \mathcal{X} and \mathcal{Y} . By denoting $\Theta = (l, A_l, (\mathbf{m}_{1,l}, \mathbf{m}_{2,l}))$, the posterior $\pi(\Theta | \mathcal{X}, \mathcal{Y})$ or $\pi(\Theta)$ for short is

$$\begin{aligned} \pi(\Theta = (l, A_l, (\mathbf{m}_{1,l}, \mathbf{m}_{2,l})) | \mathcal{X}, \mathcal{Y}) &\propto p(\Theta) p(\mathcal{X}, \mathcal{Y} | \Theta) \\ &\propto \exp(-\sigma l) \prod_{i=1}^l \left(\frac{1}{|r_{i,l}|} \right)^{n_{1i,l} + n_{2i,l}} \prod_{i=1}^l (m_{1i,l})^{\delta + n_{1i,l} - 1} \prod_{i=1}^l (m_{2i,l})^{\delta + n_{2i,l} - 1} \end{aligned} \quad (4)$$

As discussed in Section 1, a naive two-step algorithm proceeds as follows: with \mathcal{X} and \mathcal{Y} , estimating two piecewise constant densities \hat{p}_1 and \hat{p}_2 supported on (different) binary partitions independently; then computing $D_\phi(\hat{p}_1, \hat{p}_2)$, which requires to intersect all overlapped sub-regions between both partitions. The drawbacks of this type of approach are already discussed. However, according to Property 1, any two piecewise constant densities supported on different binary partitions can be rewritten such that they are defined on the same binary partition, thus we *couple* \hat{p}_1, \hat{p}_2 by partitioning their domain in tandem (i.e., forcing the same A_l) in the prior such that Theorem 1 is applicable. The divergence of \hat{p}_1, \hat{p}_2 is estimated by $\mathbf{m}_{1,l}, \mathbf{m}_{2,l}$.

3.1 Sampling

Through sampling from the posterior, the divergence are estimated by $D_\phi(\hat{p}_1, \hat{p}_2)$. According to the decomposition in (4), the depth l , the decision sequence A_l and the probability masses $\mathbf{m}_{1,l}, \mathbf{m}_{2,l}$ can be sampled hierarchically. The first step is to generate the depth l and decisions A_l . By marginalizing $\mathbf{m}_{1,l}$ and $\mathbf{m}_{2,l}$ in (4), (A_l, l) is distributed as

$$\pi(A_l, l | \mathcal{X}, \mathcal{Y}) \propto \exp(-\sigma l) \beta((\delta + n_{1i,l})_{i=1}^l) \beta((\delta + n_{2i,l})_{i=1}^l) \prod_{i=1}^l \left(\frac{1}{|r_{i,l}|} \right)^{n_{1i,l} + n_{2i,l}} \quad (5)$$

where $\beta(\cdot)$ is the multinomial Beta function and defined as $\beta((z_i)_{i=1}^k) = \prod_{i=1}^k \Gamma(z_i) / \Gamma(\sum_{i=1}^k z_i)$ and $\Gamma(z)$ is the Gamma function. Furthermore, conditioned on l, A_l is distributed as

$$\pi(A_l | l, \mathcal{X}, \mathcal{Y}) \propto \beta((\delta + n_{1i,l})_{i=1}^l) \beta((\delta + n_{2i,l})_{i=1}^l) \prod_{i=1}^l \left(\frac{1}{|r_{i,l}|} \right)^{n_{1i,l} + n_{2i,l}} \quad (6)$$

Once A_l is generated, $\mathbf{m}_{1,l}$ and $\mathbf{m}_{2,l}$ are sampled through $\text{Dir}((\delta + n_{1i,l})_{i=1}^l)$ and $\text{Dir}((\delta + n_{2i,l})_{i=1}^l)$ respectively.

It is difficult to obtain the analytical distribution of (A_l, l) because of the intractability of normalizing constant or partition function, Markov Chain Monte Carlo is employed to sample the posterior (4). However, given the vast parameter space and the countless local modes, the naive Metropolis-Hastings (Hastings, 1970) suffers from slow mixing in our experience. In order to sample effectively, a proposal kernel should be equipped with the two properties: 1) it leverages the sequential structure of binary partition and the proposed partition reflects the difference amongst sub-regions (e.g., the sample counts of \mathcal{X} and \mathcal{Y}) for rapid mixing; 2) the corresponding acceptance ratio depends on a smaller set of parameters, in other words, the transition probability is controlled by a subset of Θ , such that the size (dimensionality) of searching space is reduced. Define

$$g(\Theta' = (l', A_{l'}, (\mathbf{m}_{1,l'}, \mathbf{m}_{2,l'})) | \Theta = (l, A_l, (\mathbf{m}_{1,l}, \mathbf{m}_{2,l}))) = p(A_{l'}, l' | A_l, l) p((\mathbf{m}_{1,l'}, \mathbf{m}_{2,l'}) | A_{l'}, l)$$

where $p(A_{l'}, l' | A_l, l) = p(l' | l) p(A_{l'} | A_l, l')$ defines the jump probability, l' is constrained to be $l-1$ and $l+1$, i.e., $p(l+1 | l) + p(l-1 | l) = 1$ and $p(l-1 | l) = 0$ when $l = 1$. In order to exploit the sequential structure of binary partition such that each a_l is drawn with the guidance of A_l , $p(A_{l+1} | A_l, l+1) = p(a_l | A_l, l+1)$ is defined as

$$\begin{aligned} p(a_l | A_l, l+1) &= \frac{\pi(A_{l+1} | l+1, \mathcal{X}, \mathcal{Y})}{\pi(A_l | l, \mathcal{X}, \mathcal{Y})} \\ &\propto \frac{\beta((\delta + n_{1i,l+1})_{i=1}^{l+1}) \beta((\delta + n_{2i,l+1})_{i=1}^{l+1}) \prod_{i=1}^l |r_{i,l}|^{n_{1i,l} + n_{2i,l}}}{\beta((\delta + n_{1i,l})_{i=1}^l) \beta((\delta + n_{2i,l})_{i=1}^l) \prod_{i=1}^{l+1} |r_{i,l+1}|^{n_{1i,l+1} + n_{2i,l+1}}} \end{aligned} \quad (7)$$

and $p(A_{l-1} | A_l, l-1) = p(l-1 | l)$ since $p(A_{l-1} | A_l, l-1) = 1$, $p((\mathbf{m}_{1,l'}, \mathbf{m}_{2,l'}) | A_{l'}, l')$ is the joint Dirichlet distribution $\text{Dir}((\delta + n_{1i,l'})_{i=1}^{l'}) \times \text{Dir}((\delta + n_{2i,l'})_{i=1}^{l'})$. Thus, the acceptance ratio is

$$\begin{aligned} Q(\Theta \rightarrow \Theta') &= \min\left\{1, \frac{\pi(\Theta') g(\Theta | \Theta')}{\pi(\Theta) g(\Theta' | \Theta)}\right\} = \\ &\min\left\{1, \frac{\exp(\sigma l) \prod_{i=1}^l |r_{i,l}|^{n_{1i,l} + n_{2i,l}} p(A_l, l | A_{l'}, l') \beta((\delta + n_{1i,l'})_{i=1}^{l'}) \beta((\delta + n_{2i,l'})_{i=1}^{l'})}{\exp(\sigma l') \prod_{i=1}^{l'} |r_{i,l'}|^{n_{1i,l'} + n_{2i,l'}} p(A_{l'}, l' | A_l, l) \beta((\delta + n_{1i,l})_{i=1}^l) \beta((\delta + n_{2i,l})_{i=1}^l)}\right\} \end{aligned} \quad (8)$$

where $\pi(\Theta) = \pi(\Theta | \mathcal{X}, \mathcal{Y})$ is defined in (4). According to (8), $\mathbf{m}_{1,l}, \mathbf{m}_{1,l'}$ and $\mathbf{m}_{2,l}, \mathbf{m}_{2,l'}$ are canceled, $Q(\Theta \rightarrow \Theta')$ only depends on (A_l, l) and $(A_{l'}, l')$ which avoids searching for the vast space of $\mathbf{m}_{1,l}, \mathbf{m}_{2,l}$. Moreover, if $p(l' | l) = p(l | l')$ for $l > 1$, $Q(\Theta \rightarrow \Theta')$ can be further simplified.

In higher dimensions, sampling according to $p(A_{l'} | A_l, l')$ requires to count the number of points of \mathcal{X}, \mathcal{Y} in each sub-region of $A_{l'}$, which utilizes the information of \mathcal{X}, \mathcal{Y} but is expensive (with complexity $O((n_1 + n_2)d)$) in computation. If we are willing to run longer

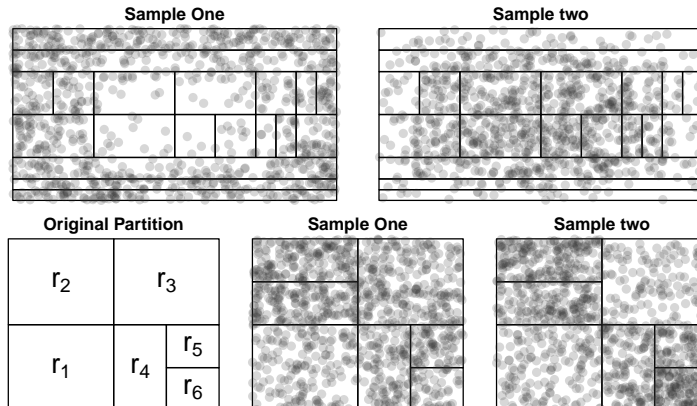


Figure 3: **Sanity Tests.** First row: 1,000 samples drawn from p_{11} and p_{21} and the learned partition; second row: 1,000 samples drawn from p_{21} and p_{22} and the learned partition.

chains with cheaper cost per iteration, another heuristic choice for transition $p(A_{l'}, l' | A_l, l)$ is to keep $p(A_{l-1}, l-1 | A_l, l) = p(l-1 | l)$ but take action a_l uniformly: $p(A_{l+1}, l+1 | A_l, l) = p(l+1 | l) / (l \cdot d)$ as there are $l \cdot d$ possible decisions (halving locations).

4 Numeric Experiments

4.1 Sanity Tests for co-BPM

We use two “sanity tests” to demonstrate that our model is sensitive to differences among samples, the densities used in experiments are two dimensional for ease of visualization. In the first group p_{11} and p_{12} , we force the mixture of p_{11} and p_{12} is uniformly distributed, i.e., $\frac{1}{2}(p_{11} + p_{12}) = \mathbf{1}\{x \in [0, 1]^2\}$; we generate 1,000 points each, thus the combined sample is equivalent to 2,000 points from uniform distribution; as shown in the first row of Figure 3, their difference is revealed by the partition well. The second group p_{21} and p_{22} are chosen such that they are both supported on the binary partition and p_{22} is defined on a finer partition than p_{21} . An effective model should be able to discover the underlying partition of p_{22} or find a partition that is finer than both p_{11} and p_{22} . The second row of Figure 3 demonstrates such effectiveness of co-BPM.

$$\begin{aligned}
 p_{11}(x) &= \frac{9}{5} \mathbf{1}\{x \in [0, 1]^2\} - \frac{4}{5} \beta_{2,2}(x_1) \beta_{2,2}(x_2) \\
 p_{12}(x) &= \frac{1}{5} \mathbf{1}\{x \in [0, 1]^2\} + \frac{4}{5} \beta_{2,2}(x_1) \beta_{2,2}(x_2) \\
 p_{21}(x) &= \frac{2}{3} \mathbf{1}\{x \in r_1\} + \frac{4}{3} \mathbf{1}\{x \in r_2\} + \mathbf{1}\{x \in r_3 \cup r_4 \cup r_5 \cup r_6\}
 \end{aligned}$$

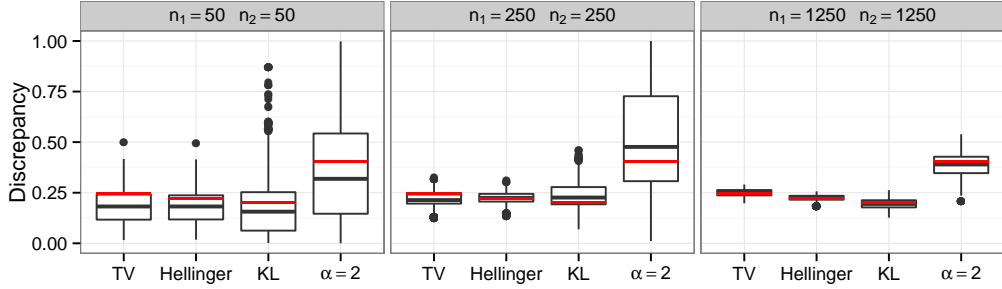


Figure 4: **1-dimensional simulation.** We draw 8,000 samples and generate box-plot after discarding the first 5,000 burn-in sample points. Theoretical divergences (red lines): 0.2461, 0.2207, 0.2000, 0.4056.

$$p_{22}(x) = \frac{2}{3}\mathbf{1}\{x \in r_1\} + \frac{4}{3}\mathbf{1}\{x \in r_2\} + \frac{1}{2}\mathbf{1}\{x \in r_3\} + \mathbf{1}\{x \in r_4\} + \frac{4}{3}\mathbf{1}\{x \in r_5\} + \frac{8}{3}\mathbf{1}\{x \in r_6\}$$

4.2 Numeric Simulations

We demonstrate our methods by 2 simulations with dimension $d = 1, 3$ and size $n_1 = n_2 = 50, 250, 1250$. The parameters for co-BPM are $\delta = 1/2$ (which is the Jeffrey’s non-informative prior), $\sigma = d + 1$, $p(l + 1|l) = p(l - 1|l) = 1/2$ for $l > 1$. The number of replicas for the box-plot is 3,000 and the burn-in number is 5,000. The divergences we consider are Total Variation, Hellinger Distance and KL divergence and α -divergence with $\alpha = 2$. The true values of the divergences are obtained by Monte Carlo method with 10^8 samples.

1-dimensional examples. The densities are defined as below and the results are summarized in Figure 4.

$$p_1(x) = \beta_{6,5}(x), p_2(x) = \beta_{5,6}(x)$$

where $\beta_{a,b}(x)$ is the Beta distribution with shape parameters a, b .

3-dimensional examples. The densities are defined as below and the results are summarized in Figure 5.

$$\begin{aligned} p_1(x, y, z) &= \frac{2}{5}\beta_{1,2}(x)\beta_{2,3}(y)\beta_{3,4}(z) + \frac{3}{5}\beta_{4,3}(x)\beta_{3,2}(y)\beta_{2,1}(z) \\ p_2(x, y, z) &= \frac{2}{5}\beta_{1,3}(x)\beta_{3,5}(y)\beta_{5,7}(z) + \frac{3}{5}\beta_{7,5}(x)\beta_{5,3}(y)\beta_{3,1}(z) \end{aligned} \quad (9)$$

It is observed from Figure 4 and 5 that co-BPM estimates the divergences reasonably well. Moreover, the estimation errors and variances are decreased when the sample size increases, so is the number of outliers in box-plots. According the histogram of depth l in Figure 5, another interesting observation is that the number of sub-regions increases in tandem with the sample size, which indicates that co-BPM refines the partitions to reveal more structure

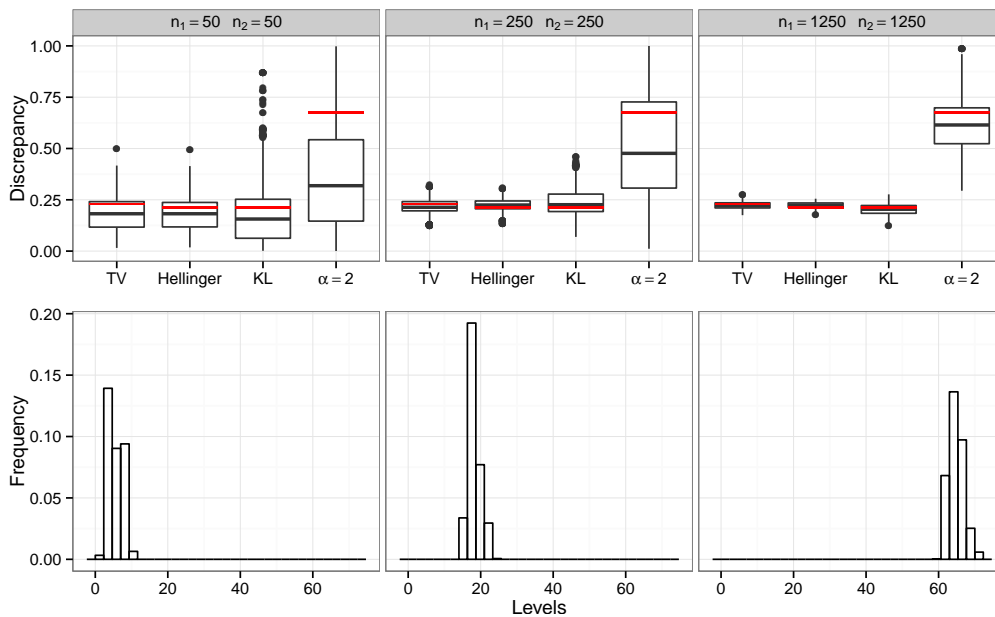
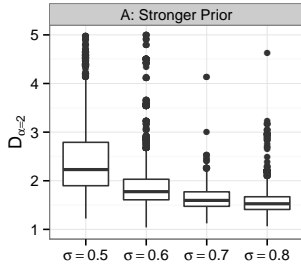


Figure 5: **3-dimensional simulation.** First row, box-plot with the same configuration as 1-dimensional case; theoretical divergences (red lines): 0.2301, 0.2129, 0.2133, 0.6769. Second row, we assess the behavior of depth l after discarding first 5,000 burn-in samples, the increase of number of sub-regions as sample size increases indicates that co-BPM refines the partitions when more information becomes available, which is analogous to the multi-resolution property discussed in (Wong and Ma, 2010).



| | Stronger Prior (δ) | | | |
|---------|-----------------------------|--------|--------|--------|
| | 0.5 | 0.6 | 0.7 | 0.8 |
| Medians | 2.3057 | 1.7771 | 1.5960 | 1.5267 |
| Std | 1.2690 | 0.6643 | 0.2223 | 0.2494 |

Table 2: **Illustration of bias and variance tradeoff.** $\mathcal{X} \sim \mathcal{N}(\mu_1 \mathbf{1}, \sigma_1^2 \mathbf{I})$, $\mathcal{Y} \sim \mathcal{N}(\mu_2 \mathbf{1}, \sigma_2^2 \mathbf{I})$ and are truncated in $[0, 1]^4$, where $|\mathcal{X}| = |\mathcal{Y}| = 500$; $\mu_1 = 1/3, \mu_2 = 1/2$ and $\sigma_1 = 1/5, \sigma_2 = 1/5$; $\mathbf{1}$ is 4-dim unit vector and \mathbf{I} is 4-dim identity matrix. As pseudo-count σ increases, the variance decreases and bias increases. True value: 2.2196. The table on the right lists the medians and standard errors.

of the sample sets as more information becomes available, this multi-resolution property of binary partition is also discussed in Optional Pólya Tree (Wong and Ma, 2010).

The vanishing boundaries of beta distribution cause the large range and variance of KL and α -divergence where division is involved, as demonstrated by the previous examples. Instead of using Jeffrey’s noninformative prior, we choose a stronger prior with larger δ as a tradeoff between bias with variance. According to law of total variance, $\text{Var}(m_{1i}) = E[\text{Var}(m_{1i}|\mathcal{X})] + \text{Var}[E(m_{1i}|\mathcal{X})]$. Since m_{1i} is generated from Dirichlet distribution, $\text{Var}(m_{1i}|\mathcal{X}) = \frac{(n_{1i}+\delta)(n_1+\delta l-n_{1i}-\delta)}{(n_1+\delta l)^2(n_1+\delta l+1)} = O(\delta^{-1})$ and $\text{Var}[E(m_{1i}|\mathcal{X})] = \text{Var}(\frac{n_{1i}+\delta}{n_1+\delta l}) = \frac{\text{Var}(n_{1i})}{(n_1+\delta l)^2}$; thus, asymptotically, its variance is reduced with a larger δ , as shown in Table 2.

4.3 Comparison with Other Methods

Most of other methods focus on KL divergence estimation. (Nguyen et al., 2010) derive a general lower bound for f -divergence via conjugate dual function; however, all of their theories and experiments are based on KL divergence estimation in 1, 2, 3 dimensions and their algorithms require that two sample sets have same size. In this section, we compare co-BPM to the methods in (Nguyen et al., 2010) and (Pérez-Cruz, 2008) in KL divergence estimation.

We briefly describe the methods in (Nguyen et al., 2010) and (Pérez-Cruz, 2008), interested readers may refer to the original papers for details. The core of (Nguyen et al., 2010)’s algorithm is a convex program that has the number of parameters equal to the sample size. As pointed out by the authors, the performance of the algorithm depends on a regularization parameter λ ; here we choose λ according to their suggestions. There are two slightly different versions of KL estimator proposed, which are denoted by NWJ-M1 and NWJ-M2 in our experiments. On the other hand, the idea of (Pérez-Cruz, 2008)’s approach, as well as (Pérez-Cruz, 2008)’s, is relatively straightforward: the k -nearest neighbor (k -NN) den-

sity estimate is computed for each sample in \mathcal{X} , i.e., $\hat{p}_1(x)$ and $\hat{p}_2(x)$ for $x \in \mathcal{X}$, then KL divergence is estimated by $\frac{1}{|\mathcal{X}|} \sum_{x \in \mathcal{X}} \log \frac{\hat{p}_1(x)}{\hat{p}_2(x)}$ (denoted by PC- k). The tuning parameter k is critical to guarantee their performance, we follow the choice of (Pérez-Cruz, 2008) by setting $k = 1$ and $k = 10$. One should also notice that the positivity of the estimates is not guaranteed as \hat{p}_1 and \hat{p}_2 are not normalized densities.

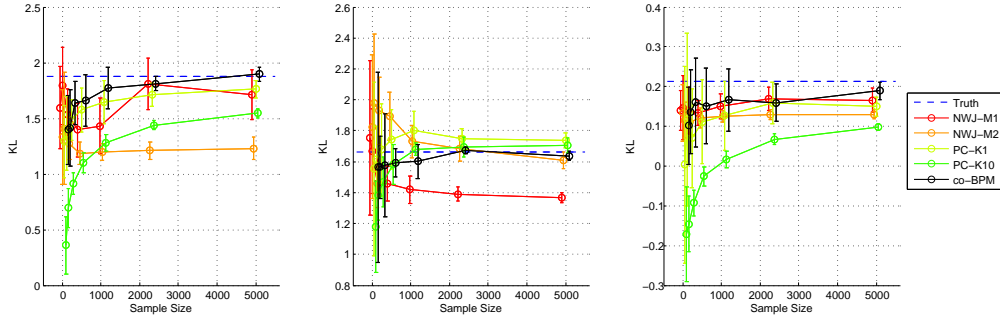


Figure 6: **Comparisons of NWJ, PC- k and co-BPM.** All densities are truncated in $[0, 1]^3$ and each line is slightly shifted to avoid overlaps. Left: $p_1(x) \sim \mathbf{1}\{x \in [0, 1]^3\}$, $p_2(x) \sim \mathcal{N}(0, (1/3)^2 \mathbf{I})$; Middle: $p_1(x) \sim \mathcal{N}(0, (1/2)^2 \mathbf{I})$, $p_2(x) \sim \mathcal{N}(1, (1/2)^2 \mathbf{I})$; Right: Beta mixture in (9).

We report their performance in Figure 6. For each of the three estimation problems described here, we experiment with 3-dim distributions and increase sample size from 50 to 5000 in logarithmic scale. Error bars are obtained by replicating each set-up 10 times. We see that co-BPM generally exhibits the best performance among the estimators considered. The estimates of NWJ-M1 and NWJ-M2 is somewhat less good and have larger variances; moreover, the convex program of NWJ-M1 or NWJ-M2 is computationally difficult because of the logarithm or entropy term and its scale increases rapidly with the sample size (Grant et al., 2008). However, PC- k is more stable than NWJ and k seems to strike a balance between bias and variance—the larger k corresponds to lower variances but larger bias, e.g., its variance is smallest when $k = 10$ in Figure 6. On the right plot, PC- k produces negative estimates with small sample size as it does not guarantee positivity.

4.4 Application to Image Clustering and Classification

As a real data example, we apply co-BPM to image clustering and classification. The images are from (Fei-Fei and Perona, 2005). Each image is segmented to a collection of local patches, where each patch is a feature vector. Assuming that each patch is an independent draw from an underlying distribution, each image is represented by an iid sample set. Hence, the dissimilarity among images can be measured by the pairwise divergences of their corresponding sample sets.

We use the same setup as in (Póczos et al., 2012): 1) we randomly select 50 images from categories “MITmountain”, “MITcoast”, “MIThighway” and “MITinsidecity” respectively; 2) features are extracted as in (Fei-Fei and Perona, 2005) and PCA is applied to reduce feature dimension to 2. The final training set has 200 sample sets (images) and each sample set contains 1600 2-dim points. We compare co-BPM with PC- k using α -divergence with $\alpha = 0.5$ and “bag-of-words” methods (BoW). BoW (Bosch et al., 2006) quantizes each patch to 100 “visual words” and uses probability latent semantic analysis to convert each image to a low dimensional (20 in our experiment) probability vector called topic distributions. The pairwise dissimilarity of images are measured by Euclidean distances.

With the dissimilarity matrices, we apply spectral clustering (Von Luxburg et al., 2008) to cluster these images. In each cluster, we define cluster-wise accuracy as the percentage of the majority category. The overall accuracy is defined as the average of all cluster-wise accuracies. The procedure is repeated 20 times and the box-plot of the accuracies are reported in the left plot of Figure 7.

α -divergence captures the difference between images pretty well. The median accuracies for co-BPM, PC- k and BoW are 83.0%, 74.9% and 72.2% respectively. The t -tests show that the difference between co-BPM and PC- k (p -value 7.97×10^{-13}) and between co-BPM and BoW (p -value $< 2.2 \times 10^{-16}$) are significant.

Using the image labels and the pairwise divergences or distances, we can predict the labels via majority vote in k -NN classification. In each run, we draw additional 100 testing images randomly. We choose $k = 9$ and repeat 20 times, their classification accuracies are summarized in the right plot Figure 7.

Similar to the results as clustering, co-BPM (77.8%) outperforms PC- k and BoW by about 3% and 5% in median accuracy. The t -test of accuracies for (co-BPM, PC- k) and (co-BPM, BoW) have p -values 9.1×10^{-4} and 8.6×10^{-6} . One possible reason that co-BPM outperforms the other two is that co-BPM is adaptive enough to discover local discrepancies like k -NN but does not suffer from the normalization issue as PC- k .

5 Conclusion and Discussion

A unified single-shot approach to estimating divergences of distributions is proposed from a Bayesian perspective. The experiments demonstrate its attractive empirical performance. In applications, this approach can be naturally extended to handle multiple-sample-set cases, i.e., we partition multiple sample sets jointly and estimate their densities as piecewise constant function on the same binary partition. Then their pairwise divergences can be computed efficiently by (3), which is useful in clustering and classification as in Section 4.4. Another direction for future work is to understand the theoretical properties of co-BPM, such as the asymptotic behavior as well as the convergence rate.

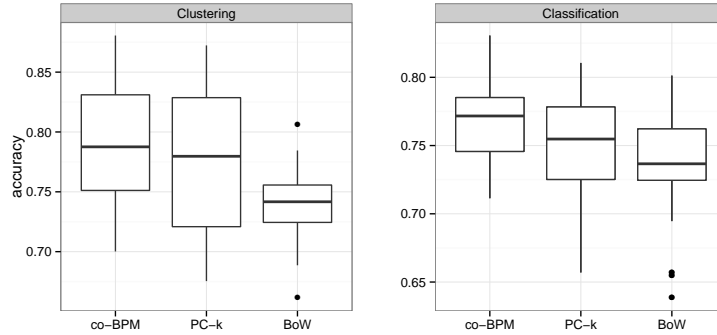


Figure 7: **Comparisons of NWJ, PC- k and co-BPM.** All densities are truncated in $[0, 1]^3$ and each line is slightly shifted to avoid overlaps. Left: $p_1(x) \sim \mathbf{1}\{x \in [0, 1]^3\}$, $p_2(x) \sim \mathcal{N}(0, (1/3)^2\mathbf{I})$; Middle: $p_1(x) \sim \mathcal{N}(0, (1/2)^2\mathbf{I})$, $p_2(x) \sim \mathcal{N}(1, (1/2)^2\mathbf{I})$; Right: Beta mixture in (9).

References

- Ali, S. and Silvey, S. D. (1966). A general class of coefficients of divergence of one distribution from another. *Journal of the Royal Statistical Society. Series B (Methodological)*, pages 131–142.
- Bosch, A., Zisserman, A., and Munoz, X. (2006). Scene classification via pls. In *European conference on computer vision*, pages 517–530. Springer.
- Chaloner, K. and Verdinelli, I. (1995). Bayesian experimental design: A review. *Statistical Science*, 10(3):273–304.
- Donoho, D. L. and Grimes, C. (2003). Hessian eigenmaps: Locally linear embedding techniques for high-dimensional data. *Proceedings of the National Academy of Sciences*, 100(10):5591–5596.
- Fei-Fei, L. and Perona, P. (2005). A bayesian hierarchical model for learning natural scene categories. In *2005 IEEE Computer Society Conference on Computer Vision and Pattern Recognition (CVPR'05)*, volume 2, pages 524–531. IEEE.
- Grant, M., Boyd, S., and Ye, Y. (2008). Cvx: Matlab software for disciplined convex programming.
- Hastings, W. K. (1970). Monte carlo sampling methods using markov chains and their applications. *Biometrika*, 57(1):97–109.

- Leonenko, N., Pronzato, L., and Savani, V. (2008). A class of rényi information estimators for multidimensional densities. *The Annals of Statistics*, 36(5):2153–2182.
- Ma, L. and Wong, W. H. (2011). Coupling optional pólya trees and the two sample problem. *Journal of the American Statistical Association*, 106(496).
- Namkoong, H. and Duchi, J. (2016). Stochastic gradient methods for distributionally robust optimization with f-divergences. *Advances in Neural Information Processing Systems*, 29.
- Nguyen, X., Wainwright, M. J., and Jordan, M. I. (2010). Estimating divergence functionals and the likelihood ratio by convex risk minimization. *Information Theory, IEEE Transactions on*, 56(11):5847–5861.
- Pérez-Cruz, F. (2008). Kullback-leibler divergence estimation of continuous distributions. In *2008 IEEE international symposium on information theory*, pages 1666–1670. IEEE.
- Póczos, B. and Schneider, J. G. (2011). On the estimation of alpha-divergences. In *International Conference on Artificial Intelligence and Statistics*, pages 609–617.
- Póczos, B., Xiong, L., and Schneider, J. (2012). Nonparametric divergence estimation with applications to machine learning on distributions. *arXiv preprint arXiv:1202.3758*.
- Sainudiin, R., Teng, G., Harlow, J., and Lee, D. (2013). Posterior expectation of regularly paved random histograms. *ACM Transactions on Modeling and Computer Simulation (TOMACS)*, 23(1):6.
- Sricharan, K., Raich, R., and Hero III, A. O. (2010). Empirical estimation of entropy functionals with confidence. *arXiv preprint arXiv:1012.4188*.
- Sugiyama, M., Kanamori, T., Suzuki, T., du Plessis, M. C., Liu, S., and Takeuchi, I. (2012). Density-difference estimation. In *NIPS*, volume 25, pages 692–700.
- Von Luxburg, U., Belkin, M., and Bousquet, O. (2008). Consistency of spectral clustering. *The Annals of Statistics*, pages 555–586.
- Wang, Q., Kulkarni, S. R., and Verdú, S. (2005). Divergence estimation of continuous distributions based on data-dependent partitions. *Information Theory, IEEE Transactions on*, 51(9):3064–3074.
- Wang, Q., Kulkarni, S. R., and Verdú, S. (2009). Divergence estimation for multidimensional densities via-nearest-neighbor distances. *Information Theory, IEEE Transactions on*, 55(5):2392–2405.
- Wong, W. H. and Ma, L. (2010). Optional pólya tree and bayesian inference. *The Annals of Statistics*, 38(3):1433–1459.